The Potential of Miniature Electrodynamic Tethers to Enhance Capabilities of Femtosatellites

IEPC-2011-054

Presented at the 32nd International Electric Propulsion Conference,
Wiesbaden • Germany
September 11 – 15, 2011

Iverson C. Bell, III[1] and Brian E. Gilchrist[2]
The University of Michigan, Ann Arbor, Michigan 48109, USA

Jesse K. McTernan[3] and Sven G. Bilén[4]
The Pennsylvania State University, University Park, Pennsylvania 16802, USA

Robert P. Hoyt[5] and Nestor R. Voronka[6]
Tethers Unlimited, Inc. Bothell, Washington 98011, USA

and

Mason A. Peck[7]
Cornell University, Ithaca, New York 14853, USA

In this paper we investigate an approach that appears to scale to the small size needed for femtosatellite (commonly called "ChipSats") drag make-up and even orbit raising with the added benefit of being propellantless. The approach uses a short, semi-rigid electrodynamic tether (EDT) for propulsion, which keeps the overall ChipSat mass low and provides enough thrust to overcome drag in LEO. We report on our trade studies to assess the feasibility of using the EDT for ChipSat propulsion. We have analyzed the EDT anode's ability to draw current from the ionosphere and thereby generate thrust. We then traded this performance against the tether mass and material, electron emitter and collector types, and power needed to determine the EDT's capability of overcoming atmospheric drag forces. The study led to the development of a system concept and mission scenario using the simulation tool TeMPEST to estimate tether voltages and currents based on tether configuration and ambient ionosphere and atmosphere models. The results reveal that an insulated tether only a few meters long and tens of microns in diameter could provide milligram to 100 gram-level ChipSats with complete drag cancellation and even the ability to change orbit. A more complete systems design and analysis is continuing.

Nomenclature

A = Ram spacecraft cross section area (m^2)
A_{EDT} = Tether cross section area (m^2)

[1] Ph.D. Candidate, Electrical Engineering, icbell@umich.edu.
[2] Professor, Electrical Engineering and Computer Science, gilchrst@eecs.umich.edu.
[3] Graduate Student Research Assistant, Aerospace Engineering, jkm249@psu.edu.
[4] Assoc. Professor, Engineering Design, Electrical Engineering, and Aerospace Engineering, sbilen@psu.edu.
[5] CEO and Chief Scientist, hoyt@tethers.com.
[6] VP and Chief Technologist, voronka@tethers.com.
[7] Associate Professor, Mechanical and Aerospace Engineering, MP336@cornell.edu.

A_{sun} = Area exposed to the sun (m^2)
a = Semi-major axis (m)
a_{accel} = Acceleration (m/s^2)
a_{FN} = Fowler–Nordheim current coefficient ($A \cdot V^{-2}$)
$\mathbf{B}$ = Magnetic field (T)
b_{FN} = Fowler–Nordheim voltage coefficient (V)
C_d = Drag coefficient, 2.2
c = Speed of light in a vacuum, 2.99×10^8 $m \cdot s^{-1}$
E = Modulus of elasticity (Pa)
F_T = Drag force on the satellite (N)
F_e = Drag force on the tether (N)
H = Atmospheric density scale height (m)
$I_{inertia}$ = Tether area moment of inertia (m^4)
$\mathbf{I}_{spacecraft}$ = Spacecraft mass moment of inertia ($kg \cdot m^2$)
I_{tether} = Tether current (A)
k Boltzmann constant, 1.38×10^{-23} J/K
L = Tether length (m)
M = Moment ($N \cdot m$)
m = Total mass (kg)
m_{EDT} = Tether mass (kg)
m_e = Electron rest mass, 9.1×10^{-31} kg
$m_{endbody}$ = Satellite mass (kg)
P_{drag} = Pressure from atmospheric drag, $\frac{1}{2} C_d \rho v^2$ ($N \cdot m^{-2}$)
q = Elementary charge, 1.6×10^{-19} C
R = Electrical resistance (Ω)
R_0 = Distance from spacecraft center of mass to the Earth's center (m)
r = Tether radius (m)
r_d = Distance traveled (m)
r_{probe} = Radius of plasma probe (m)
$\mathbf{S}_{cp}$ = Vector distance from center of mass to center of pressure (m)
T_e = Electron temperature (eV)
t_{in} = Tether insulator thickness (m)
$\mathbf{u}_e$ = Unit vector to nadir
V_{gate} = Cathode base-gate voltage
v = Velocity (m/s)
W = Work ($N \cdot m$)
β = Ratio of probe radius to attracted particle gyroradius
$\Gamma_{diffuse}$ = Diffuse coefficient of reflectivity
Γ_{spec} = Specular coefficient of reflectivity
ε = Ratio of maximum tether deflection to total tether length
$\eta_{anode\text{-}fraction}$ = Ratio of anode power to available power
$\eta_{conversion}$ = DC–DC conversion efficiency
$\eta_{SP\text{-}efficiency}$ = Solar panel efficiency
μ = Standard gravitational parameter of Earth, 3.986×10^{14} $m^3 \cdot s^{-2}$
ρ = Atmospheric neutral density ($kg \cdot m^{-3}$)
ρ_{EDT} = Tether conductor mass density ($kg \cdot m^{-3}$)
$\rho_{resistivity}$ = Electrical resistivity (Ω m)
Φ_p = Probe potential (V)
Φ_{direct} = Direct solar radiation flux ($W \cdot m^{-2}$)
Φ_{albedo} = Earth albedo of direct solar flux ($W \cdot m^{-2}$)
ψ = Ratio of probe potential to plasma potential

I. Introduction

The growing success of and interest in nanospacecraft (1–10 kg) over the past decade has generated interest in exploring the potential for even smaller spacecraft, both as stand-alone satellites or as a distributed *swarm.*[1–3]

Because of advances in integrated circuit and microelectromechanical systems (MEMS) technology, the feasibility of miniaturized spacecraft at the levels of fully monolithic semiconductor integrated circuits (10–100 mg) or hybrid integrated circuits (10–100 g) is being seriously investigated.[4–6] ChipSats belong to the picosatellite (100 g–1 kg) and femtosatellite (<100 g) mass categories. Effectively, this architecture can be thought of as a small "satellite-on-a-chip" or "ChipSat".

Because of their low masses and small sizes, they are orders of magnitude less costly to manufacture, test, and boost into orbit. Large groups of reconfigurable satellites also present unique mission capabilities, such as simultaneous, distributed data collection; ad hoc in-space data relay networking; and enhanced communication via configuration as an antenna array.

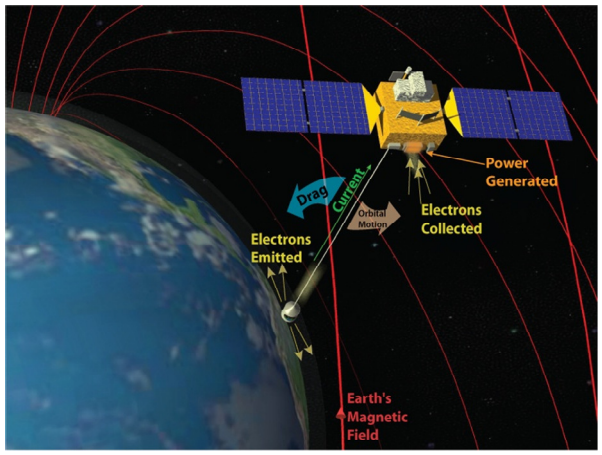

Figure 1. Illustration of electrodynamic tether operating, attached to a larger sized spacecraft in orbit.

Flat ChipSat wafers, however, have an inherently high area-to-mass ratio. Although this feature can be exploited for new behaviors, it can result in an undesirably short orbital lifetime in low Earth orbit (LEO) due to atmospheric drag, ranging from a few days to a few hours depending on altitude and solar conditions. While a satellite using chemical propulsion can overcome the continuous force of atmospheric drag, the volume of propellant required will increase with the satellite's intended lifetime. Thus, the use of a traditional thruster with propellant and need for directed flow to compensate for drag and possibly for maneuverability would increase the size, mass, and complexity of ChipSats. The need for ChipSat maneuverability is especially important considering the technology's capability for swarm missions that might require a high degree of orbital maintenance. The small size of the satellites also presents a challenge for energy storage, communication, and tracking.

In this paper, we investigate an approach that appears to scale to the small size needed and is also propellantless. The approach uses a short, semi-rigid electrodynamic tether (EDT) for propulsion, which keeps the overall ChipSat mass low and provides enough thrust to overcome drag in LEO. An EDT exploits the Lorentz force to generate thrust for boost, deboost, and inclination change, using current in a conducting tether to produce a force in the presence of the Earth's magnetic field. The Lorentz force is expressed as[8]

$$\mathbf{F}_{\text{Lorentz}} = \int_0^L (I_{\text{tether}} d\mathbf{L}) \times \mathbf{B} \qquad (1)$$

and the magnitude of the force is

$$F_{\text{Lorentz}} = I_{\text{tether}} L B \qquad (2)$$

for a straight, insulated tether oriented perpendicular to the magnetic field.

The tether circuit is closed by collecting charge from the Earth's ionosphere at one end and emitting charge of the same sign or collecting charge of the opposite sign at the other end, with final closure occurring in the surrounding plasma. This process is illustrated in Fig. 1.

We report on our trade studies to assess the feasibility of using the EDT for ChipSat propulsion. We have analyzed the EDT anode's ability to draw

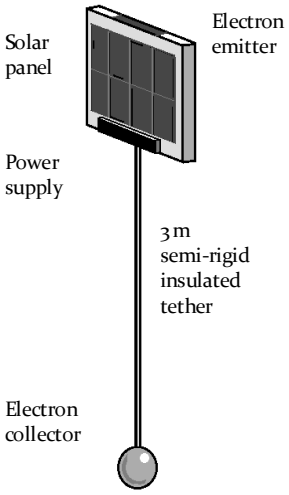

Figure 2a. Early ChipSat EDT concept.[7]

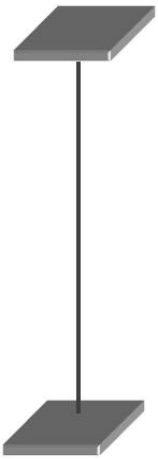

Figure 2b. Advanced ChipSat EDT concept. Each end-body has a solar panel, power supply, and an electron emitter and is capable of collecting electrons on the surface.

current from the ionosphere and through the tether, thereby generating thrust, and have traded this performance against the tether mass and material, tether rigidity, and power needed to determine the EDT's capability of overcoming atmospheric drag forces. The study led to the development of a system concept and mission scenario using the simulation tool TeMPEST to estimate tether voltages and currents based on tether configuration and ambient models. TeMPEST incorporates current geomagnetic field models, ionospheric and atmospheric conditions, plasma contactor modeling, and precise orbital calculations.

The system concept developed in the previous trade study,[7] shown in Fig. 2a, is capable of drag make-up and boost. The ChipSat is also oriented so the maximum cross-sectional area is perpendicular to velocity. Figure 2b shows the more advanced system concept investigated in this trade study. This system has the capability to boost, deboost, and collect solar energy with the upper and lower end-bodies. The satellite is oriented so the minimum cross-sectional area is perpendicular to velocity. We designed the satellite–tether symmetry to position the center of pressure, the center of mass, and the center of gravity roughly at the same location midway along the tether. This

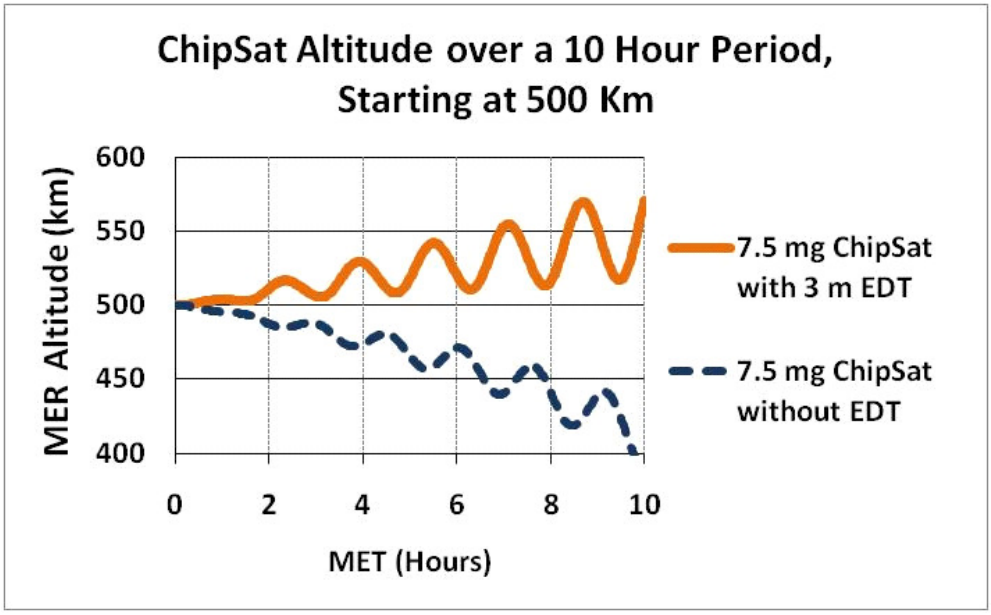

Figure 3. TeMPEST simulation results of ChipSat orbit with and without the electrodynamic tether.

should help reduce torque introduced by atmospheric drag.

The results from the previous trade study,[7] shown in Fig. 3, reveal that an insulated tether only a few meters long and tens of microns in diameter can provide milligram- to 100 gram-level ChipSats with complete drag cancellation and even the ability to change orbit. Additional details on the trade study's assumptions and calculations may be found in Ref. 7.

II. Trade Study

A. Ionosphere/Atmosphere Environment

The conditions of the atmosphere and ionosphere heavily influence EDT performance. The current in the tether, I_{tether}, scales with electron density. The peak electron density, and thus EDT thrust capability, occurs in the F2 region of the ionosphere between 300 and 500 km. We assume a 500-km circular orbit. We also assume a low inclination orbit to ensure that the thrust in Eq. (1) is primarily in-plane for a tether oriented along the local vertical.

We conducted the trade study during high solar activity, when the neutral-to-electron-density ratio is an order of magnitude higher than at low solar activity. The force of atmospheric drag counters orbital velocity and reduces the altitude of an orbiting body over time. The expression for atmospheric drag force is given by

$$\mathbf{F}_{\text{drag}} = -\tfrac{1}{2}\rho C_d A v^2 \hat{\mathbf{v}} \tag{3}$$

and torque due to drag is given by[9]

$$\boldsymbol{\tau}_{\text{drag}} = \mathbf{F}_{\text{drag}} \times \mathbf{S}_{\text{cp}} . \quad (4)$$

The drag force scales with the neutral density and the thrust scales with electron density, so the elevated neutral-to-electron-density ratio during high solar activity actually represents the worst case scenario for thrusting at 500 km.

We determined the electron density by averaging the densities calculated at 500 km altitude at the equator during the solar high of solar cycle 23 (July 2000[10]) using the International Reference Ionosphere-2007 (IRI-2007) model. The neutral density was similarly taken from the Mass-Spectrometer-Incoherent-Scatter (MSIS-E-90) model. Atmosphere and ionosphere assumptions are summarized in Table 1.

Table 1. Ionospheric conditions.

Parameter	Value
Altitude	500 km (circular)
Spacecraft Velocity (relative to co-rotating atmosphere)	7.5 km·s^{-1}
F10.7 (solar activity)	169 (Solar High)
Electron Temperature	0.15 eV
Magnetic Field	0.3 gauss
Gyroradius	3 cm
Neutral Density	1x10^{-15} g·cm^{-3}
Electron Density	5×10^{5} electrons·cm^{-3}
Debye Length	4 mm
Electron-to-neutral Density	1×10^{22} electrons·g^{-1}

B. Orbital Lifetime

The atmospheric drag force is the dominant non-gravitational force in LEO. The change in semi-major axis due to atmospheric drag is given by[9]

$$\Delta a_{\text{revolution}} = 2\pi\left(\frac{C_d A}{m}\right)\rho a^2 , \quad (5)$$

which scales with the satellite's area-to-mass ratio. The orbital lifetime

$$\text{Lifetime} \approx \frac{H}{\Delta a_{\text{revolution}}} \quad (6)$$

is roughly proportional to the inverse of this ratio, or the ballistic coefficient. Figure 4 illustrates that smaller femtosatellites have lower ballistic coefficients. The estimated lifetimes of the satellites in Fig. 2 in LEO range from years for the Surrey SpaceChip[4] to days for the Cornell MCM Sat.[5] In order to make formation flying more feasible and to extend the orbital lifetime of the spacecraft, there is a strong benefit for a propulsion system that scales to the size of the satellites without significantly increasing the satellites' on-board mass, power, or complexity.

C. Trade Study Satellites

The satellites in the trade study roughly span the mass and ballistic coefficient range represented by actual pico- and femtosatellites, as shown in Fig. 4. The mass and size of the largest satellite in the trade study (100 g) was motivated by the DARPA/Aerospace Corporation satellites PicoSat 1 and 2. PicoSats 1 and 2 were identical 250-g satellites connected by a 30-meter tether. They were launched in January 2000.[6]

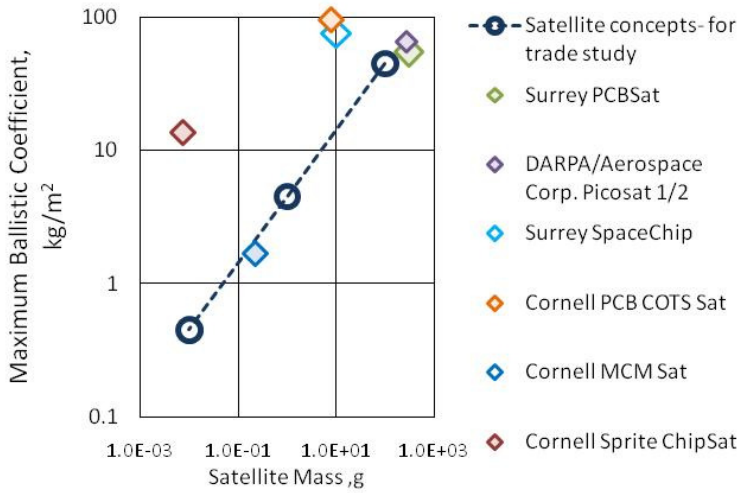

Figure 4. Ballistic coefficient for a range of ultra-small satellites assuming the smallest area cross-section.[4,5,6]

The mission demonstrated RF-MEMS in space. Each PicoSat was equipped with a radio and could communicate to the other satellite and to the ground. The Picosats could also be successfully tracked because the

Table 2. Parameters for satellites used in the trade study.

Satellite concept for trade study	Dimensions	Mass	Cross section area	Drag force, 500-km altitude	Orbital lifetime estimate, 500-km initial altitude
Large femtosatellite	2 cm×5 cm×5 cm	100 g	10 cm^2	60 nN	few years
Medium femtosatellite	1 cm×1 cm×1 cm	1 g	1 cm^2	6 nN	few months
Small femtosatellite	1 mm×1 cm×1 cm	10 mg	0.1 cm^2	0.6 nN	few days

tether connecting the PicoSats had a thin gold wire strand that increased the radar cross section of the structure. The ground antenna tracking the satellites was a 150-ft-diameter (45.7-m) parabolic antenna.[11]

The smallest satellite considered in the study, the 10-mg satellite, was motivated by the Sprite ChipSat.[5] The Sprite ChipSat is currently undergoing testing on the Materials International Space Station Pallet on the International Space Station. The 1-g femtosatellite bridges the mass and ballistic coefficient gap between the higher and lower mass satellites. Information on the satellites used in the trade study is provided in Table 2.

D. Tether Material Composition

The tether for a miniaturized EDT will have different requirements than tethers used for more massive satellites. In an EDT system for larger spacecraft, one satellite, or end-body, deploys a second end-body and the two are connected by a tether cable that can range from a few hundred meters to tens of kilometers in length. We expect a tether for femtosatellites to be much shorter. The end-bodies for traditional EDT systems are also orders of magnitude larger and more massive than considered here. For example, in the Tethered Satellite System (TSS) missions, the Space Shuttle, which has a mass of about 100,000 kg, deployed a 521 kg, 1.6-m diameter sphere as the second end-body.[12] In this case, the gravity-gradient force generated tension along the tether, pulling the long cable along the local vertical. The approximate gravity gradient force is given by[9]

$$F_{\text{gravity-gradient}} \approx \frac{3m\mu L}{R_0^{\,3}} \tag{7}$$

and the corresponding torque is given by

$$\boldsymbol{\tau}_{\text{gravity-gradient}} = \frac{3\mu}{R_0^{\,3}} \mathbf{u}_e \times \left(\mathbf{I}_{\text{spacecraft}} \bullet \mathbf{u}_e \right). \tag{8}$$

The gravity gradient force can orient long objects along the local vertical. This orientation is important because a tether that is aligned along the local vertical in a low inclination orbit in LEO can generate peak in-plane thrust.

In our design, we assume the end-bodies are identical femto- or picosatellites of equal size and mass since current collection and emission must occur at each end of the tether. The vertical symmetry also helps improve the ability to have the center of mass, center of gravity, and the center of pressure located roughly at the midway point along the tether. This should help reduce any torques induced by atmospheric drag, like that given in Eq. (4). The gravity-gradient force given by Eq. (7), which scales with mass and length, will be small for femtosatellites. As a result, a more rigid material is required to ensure that the tether achieves near straight orientation regardless of forces along its length or on the end-bodies, e.g., drag or solar pressure. On a long time scale, if the tether acts like a rigid beam, the gravity-gradient torque in Eq. (8) should align it in the local vertical assuming symmetry in the system. This last assumption requires additional investigation.

We have designed the EDT to have a semi-rigid, conducting metal core and a thin layer of insulation. We chose Kapton™ to be the insulation material due to its common use as spacecraft insulation and its high breakdown potential. The tether insulation is 2 μm thick. In the case that the anode bias voltage approaches the breakdown potential for 2-μm insulation, we instead use 4 μm of Kapton.

Table 3. Properties of tether materials used for the trade study.

Material Property	Value
Monel K-500[13]	
Electrical resistivity (21 °C)	6.15×10^{-7} Ω·m
Mass density	8.47 g·cm^{-3}
Elastic Modulus, Tension	179 GPa
Kapton film[14]	
Dielectric Strength	291 V·μm^{-1}
Mass density	1.54 g·cm^{-3}

We chose Monel-K500 to be the EDT core because of its high Young's modulus and yield strength. Although Monel™ is not a good conductor, the tether lengths and currents are small enough that the resistance, given by

$$R = \rho_{\text{resistivity}}\left(\frac{L}{A}\right), \tag{9}$$

is not high. Furthermore, the power dissipated in the tether is not a dominant factor because this loss term scales with resistance and the square of current, both of which are small values. Some properties of Kapton film and Monel-K500 are included in Table 3.

E. Tether Rigidity and Radius

The force of atmospheric drag can bend or bow a tether because the magnitude of this force can vary between the tether and the end-bodies. Sufficient bowing reduces the vertical length of the tether, which in turn can reduce thrust from that in Eq. (2). To investigate tether bowing due to drag, we use D'Alembert's principle to transform the accelerating body into a static system by adding inertial forces and torques. This technique allows us to solve for EDT deflection as we would solve for deflection along a simply supported beam.[15] The details of the derivation may be found in the Appendix. The variation in drag force along the structure causes a maximum deflection at the center calculated by

$$y_{\max} = -\frac{10L^3 P_{\text{drag}}}{384EI_{\text{inertia}}}\left(\frac{A_{\text{EDT}}m_{\text{endbody}} - Am_{\text{EDT}}}{2m_{\text{endbody}} + m_{\text{EDT}}}\right). \tag{10}$$

The deflection $y_{\max}$ in Eq. (10) gives the bowing distance, which is the distance the center of the tether moves relative to the end-bodies. The zeros of Eq. (10), or tether radii that cause $y_{\max} = 0$, cannot be used because the radii are either extremely small (sub-micron) or large (millimeter). Alternatively, we can solve for a radius in Eq. (10) that limits tether bowing to a small distance. We solve Eq. (10) by limiting the maximum deflection to the total length multiplied by a small number ε, i.e., $y_{\max} = \varepsilon L$. For example, if $\varepsilon = 0.01$ for a 1-m tether, the tether center bends outward 1 cm from both ends. Equation (10) can be rearranged to give the atmospheric drag pressure

$$P_{\text{drag}} = \varepsilon 38.4\frac{EI_{\text{inertia}}}{L^2}\left(\frac{2m_{\text{endbody}} + m_{\text{EDT}}}{A_{\text{EDT}}m_{\text{endbody}} - Am_{\text{EDT}}}\right). \tag{11}$$

We rewrite Eq. (11) as

$$\frac{1}{2}C_d\rho v^2 = \varepsilon 38.4\frac{E\left(\frac{\pi}{4}(r - t_{\text{in}})^4\right)}{L^2}\left(\frac{2m_{\text{endbody}} + \left(\rho_{\text{EDT}}L\pi(r - t_{\text{in}})^2\right)}{2rLm_{\text{endbody}} - A\left(\rho_{\text{EDT}}L\pi(r - t_{\text{in}})^2\right)}\right) \tag{12}$$

in order to solve for the radius of the tether. One should note that the radius depends on ambient conditions.

Figure 5 shows the radii for tether stiffness for a range of tether lengths. It is important to note that, in the remainder of the trade study, we calculate parameters for each satellite such as drag, current, and power using the EDT radii in Fig. 5 that make the tether stiff at a given length. For example, a 10-m-long EDT designed for a 100-g satellite ($\varepsilon = 0.01$, $r = 106$ μm) has a different radius than a 1-m-long EDT designed for the same satellite ($\varepsilon = 0.01$, $r = 24$ μm). However, both tethers bow outwards a maximum of 1% the total length due to atmospheric drag. The insulator is very thin and flexible relative to the metal core, so we assume that the Monel core provides the rigidity.

We assume that lateral deflection where $\varepsilon = 0.01$ is sufficient to treat the tether and satellites as a single rigid structure. To illustrate the impact of the relationship between radius and required current, we write Eq. (2) as

$$I_{\text{tether}} = \frac{F_{\text{drag}}}{LB} = \frac{\frac{1}{2}c\rho v^2(2A + 2Lr)}{LB}. \tag{13}$$

The current required for drag make-up scales with tether length and radius. Stiffer tethers have larger radii and, consequently, a higher drag force and required current. Thus, if one designs an EDT with a large radius to further increase stiffness, the system requires more current to overcome the elevated drag force.

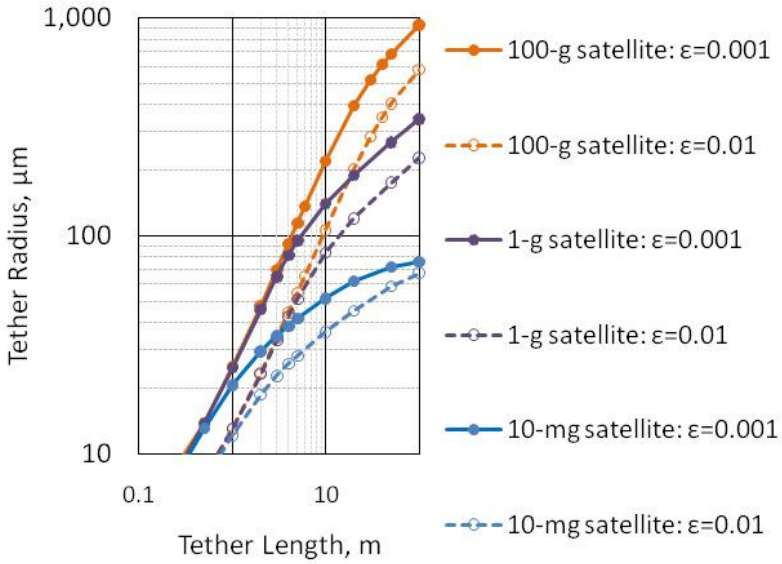

Figure 5. Minimum radius for tether rigidity.

F. Tether Mass

The tether mass can be calculated for a given length by

$$m_{EDT} = \rho_{EDT} L \pi r^2 \tag{14}$$

using the tether radii found in Fig. 5 and the material densities found in Table 3. The mass reported in Fig. 6 shows the mass of the tether and the mass of the satellite. The lower end-body is a femtosatellite, so the total mass of the system is the sum of the tether mass and twice the satellite mass.

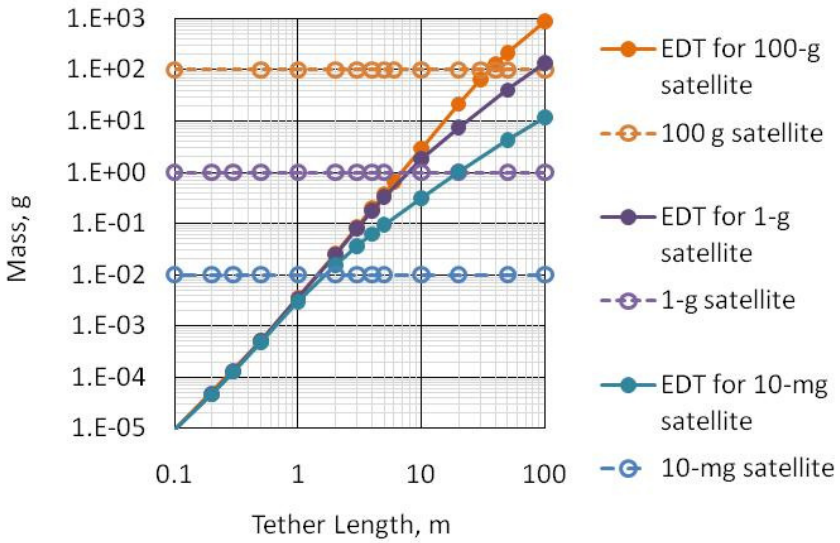

Figure 6. Tether and satellite mass.

G. Tether Current

1. Anode current

EDT thrust is proportional to current. Due to the higher mobility of electrons, more electron current may be collected per unit area than ion current. Electrons can be collected on the outer surfaces of the satellites. We assume that the femtosatellites can be coated with a transparent conductor, e.g., indium tin oxide, to facilitate the needed low current collection. For the 1-g and 10-mg femtosatellite, we can roughly estimate the current by approximating the satellite to be a sphere with a diameter equal to each satellite's largest dimension or diagonal. The diagonals of the 10-mg and 1-g satellites are about 3 Debye lengths For an anode at a high bias with respect to plasma potential ($\sim\Phi_p > 100T_e$ or 15 V), we expect the sheath to extend outwards several Debye lengths into the plasma and shield out the precise probe geometry.

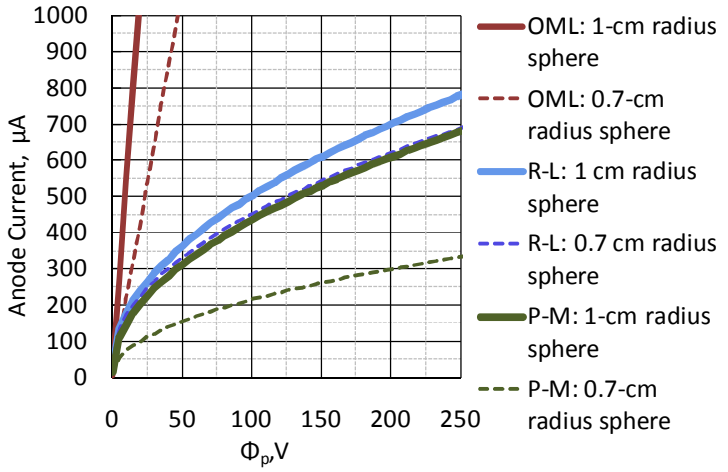

Figure 7. Current-voltage characteristic for a 1-cm radius sphere (β = 0.32) and a 0.7-cm radius sphere (β = 0.23). Table 1 plasma density is used.

We conservatively estimate current collected by the 100-g satellite by assuming all four 2-cm-high edges of the satellite collect current like a single 2-cm-diameter sphere. The six faces should collect current like flat plates, but the current collection on these surfaces is small. We also ignore collection along the eight 5-cm satellite edges. It should be noted that this estimate may be too conservative and should be analyzed further.

The Rubinstein–Laframboise (R–L) canonical upper bound current can estimate current collected by a biased spherical probe in a weakly magnetized plasma. The R–L current is given by[16]

$$I_{\mathrm{R-L}} = I_{\mathrm{tether}} = I_{\mathrm{thermal}}\left(\frac{1}{2} + \frac{2\sqrt{\psi}}{\beta\sqrt{\pi}} + \frac{2}{\beta^2\pi}\right),\ \psi \to \infty, \tag{15}$$

where the thermal current is

$$I_{\mathrm{thermal}} = 4\pi r_{\mathrm{probe}}^2 n_e q\sqrt{\frac{kT_e}{2\pi m_e}}\,. \tag{16}$$

Equation (15) is an approximation of the R–L current that assumes $\Phi_p >> T_e$. Figure 7 shows the R–L current–voltage (I–V) curve relative to the orbital motion limited[17] (OML) and Parker–Murphy[18] (P–M) I–V curves. The Parker–Murphy theory is appropriate when the probe-radius-to-gyroradius ratio, or β, far exceeds the β for small satellites in LEO. Thus, we expect to collect much more current at a given voltage than this theory and less than the maximum allowable current estimated by OML theory. The R–L I–V curve lies between the OML and P–M curves, so it is our best estimate.

2. Cathode current

Field emitter array (FEA) technology can be used to emit electrons at the opposite end of the tether. The Fowler–Nordheim emission law[19] is

$$I_{\mathrm{cathode}} = a_{FN} V_{\mathrm{gate}}^{\ 2} \exp(-b_{FN}/V_{\mathrm{gate}})\ . \tag{17}$$

The Spindt cathode consists of an array of sharp-tipped, sub-μm-radius cones that emit electrons when the nearby gate is biased to V_{gate}. Carbon nanotube emitter arrays may be a feasible alternative for future femtosatellites. A minimum current is noticeable at specific EDT lengths in Fig. 5: the current minimum is 1 meter for the 10-mg

satellite, 3 meters for the 1-g satellite, and 10 meters for the 100-g satellite. We calculate the maximum available current, shown in Fig. 8, from available power, which we discuss in Section H.

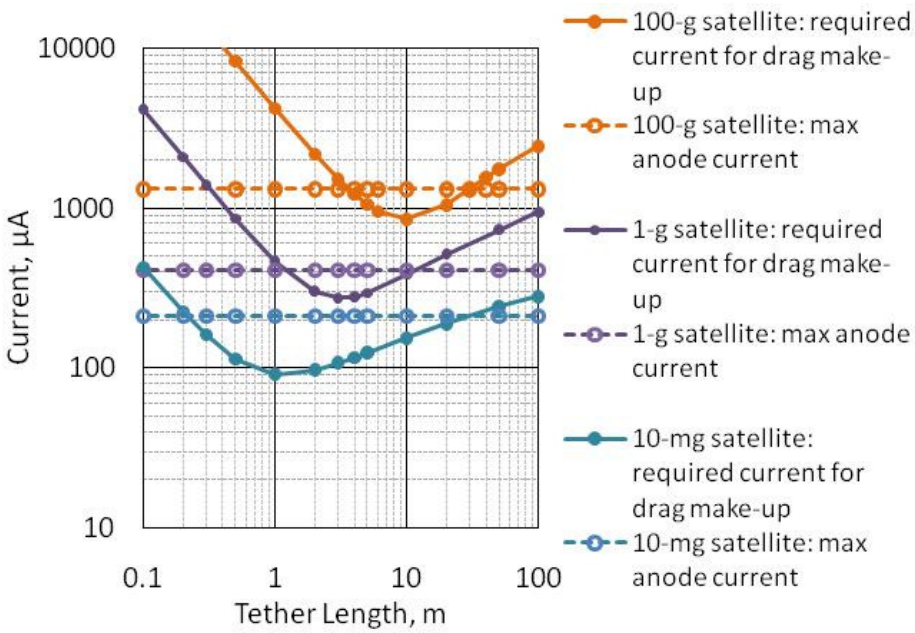

Figure 8. Required current for rigid tether ($\varepsilon = 0.01$).

H. Power

In order to determine if EDT propulsion is feasible for femtosatellites, the electrical power used by the EDT system to overcome the drag force must be less than the generated power.

1. *Generated power*

We estimate the amount of electrical power generated by the satellite with the expression

$$P_{\text{generated}} = \frac{1}{2}\eta_{\text{SP-efficiency}}\left(A_{\text{sun}}\phi_{\text{direct}} + A_{\text{sun}}\phi_{\text{albedo}}\right) . \tag{18}$$

We assume that the femtosat has solar panels on all six sides of the upper and lower end-bodies, three of which are exposed to the sun at any given time. The solar panel has an efficiency $\eta_{\text{SP-efficiency}}$, which we assume to be 10% as reported in Ref. 20. Of the total energy collected from direct solar radiation and Earth albedo, we assume that 25% is lost in the step-up voltage DC–DC converter and other loads. We neglect the small energy contribution from Earth infrared radiation. The expression estimating generated power also assumes that the satellite is in the sun roughly half of the time, i.e., the ½ coefficient. The actual amount of time in the sun depends on the orbit and the altitude.

2. *Dissipated power*

The power required for EDT thrust is

$$P_{\text{total}} = P_{\text{tether}} + P_{\text{anode}} + P_{\text{cathode}} . \tag{19}$$

The power required to collect electrons is a fraction of the total available power, given by

$$P_{\text{anode}} = \eta_{\text{anode-fraction}} P_{\text{generated}} , \tag{20}$$

and it can be calculated by

$$P_{\text{anode}} = I_{\text{R-L}}\Phi_p . \tag{21}$$

The power required to emit electron current from the cathode is

$$P_{\text{cathode}} = I_{\text{anode}} V_{\text{gate}} . \tag{22}$$

The power dissipated in the tether, given by

$$P_{\text{tether}} = I_{\text{tether}}^2 R , \tag{23}$$

is small relative to other losses because the current and resistance are low.

To solve for maximum available current, we assume that some fraction $\eta_{\text{anode-fraction}}$ of the overall generated power is reserved for current collection. The maximum current and anode potential can be calculated from Eq. (20) and Eq. (13). We then find the FEA base-gate potential V_{gate} required to emit the collected current and calculate the power needed to operate the cathode.

The electromotive force is a loss mechanism for boosting in low inclination prograde orbits, but we disregard it in Eq. (19) because it is extremely small for the tether lengths considered. Current and power are directly related, so given the shape of the current–tether length curve in Fig. 8, we expect a similar shape for the power–tether length curve in Fig. 9. A short EDT requires a large current to overcome the drag force on the satellite. The rigidity of a beam decreases with length, so a very long EDT must have a large radius to prevent bowing. As a result, the drag due to the tether dominates over the drag due to the satellite, driving up the required current. The current is minimized when these two effects are balanced. Table 4 summarizes the power calculations.

Figure 9 shows the available power for thrust and the required thrust power. The available power is the estimated power available for EDT propulsion after DC–DC converter loss and loss to other loads. The required thrust power is the power needed to overcome the atmospheric drag force. If the required thrust power is higher

than the available power, the EDT cannot overcome the drag force. However, if the converse is true and the femtosatellite has more power available than is required for thrust, the EDT can boost.

Table 4. Power constraints for current collection.

Parameter	10-mg satellite	1-g satellite	100-g satellite
Solar radiation flux ($W \cdot m^{-2}$)	1367	1367	1367
Earth albedo (%)	30	30	30
Solar panel area exposed to the sun (cm^2)	2	6	90
Total generated power (mW)	17	53	800
Power available for propulsion after 25% is lost to DC–DC conversion and other loads (mW)	13	40	600
Anode power (mW)	3.7	21	540
Equivalent anode sphere radius (cm)	0.7	0.86	1
Anode voltage (V)	17	52	430
Anode current (μA)	214	403	1250
Cathode power (mW)	8.5	16.7	56.6
Cathode base-gate voltage (V)	39.6	41.4	45.12
Power dissipated by tether (mW)	0.01	0.04	0.5
Total power consumed (mW)	12.2	37.7	596

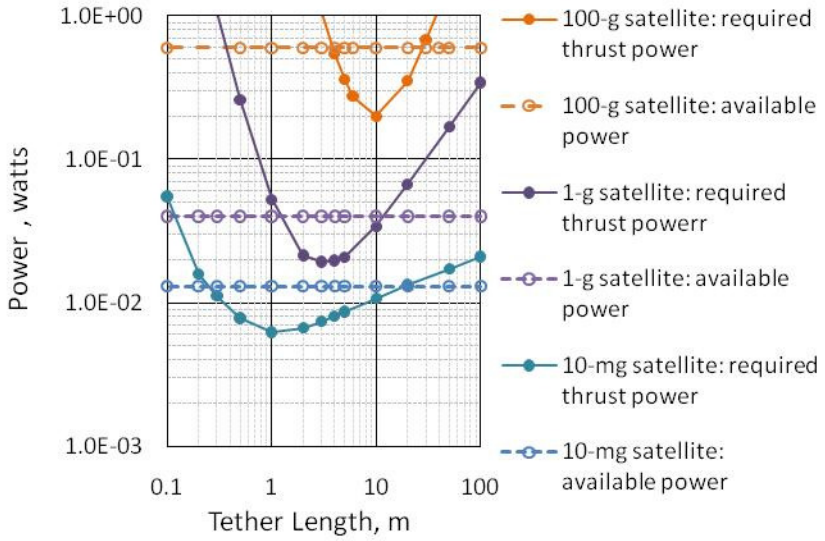

Figure 9. Electrical power required for drag make-up thrust and available electrical power.

I. Estimating Forces on the Tether and the Femtosatellite

The drag force, the solar radiation pressure force, the gravity gradient force, and the Lorentz force are the dominant forces acting on the femtosatellites and tether system in LEO. The drag force is given by Eq. (3), the gravity gradient force is given by Eq. (7), and the Lorentz force is given by Eq. (2). To estimate the solar radiation pressure force, we calculate the maximum force on each end-body as

$$F_{\text{plate}} = \frac{A\Phi_{\text{direct}}}{c}\left[\left(1-\Gamma_{\text{spec}}\right)+2\left(\frac{\Gamma_{\text{diffuse}}}{3}+\Gamma_{\text{spec}}\right)\right] \tag{24}$$

and the maximum force on the tether as

$$F_{\text{cylinder}} = \frac{2\pi rL\Phi_{\text{direct}}}{3c}\left[\frac{1+\Gamma_{\text{spec}}}{\pi}+\frac{\Gamma_{\text{diffuse}}}{2}\right] \tag{25}$$

and sum the quantities, assuming they simply add. Equations (24)[21] and (25)[21] are both maximum forces where the solar radiation is directly incident on the surface, i.e., there is no tilt angle between the surface normal and the incident solar radiation. The total solar radiation pressure force, shown in Figs. 10–12, is the sum of Eq. (24) and Eq. (25). We do not calculate the torque due to the solar radiation pressure force.

Table 5. Representative solar panel and Kapton optical properties.

Parameter	Kapton H Film[22]	Solar Panel[23]
Γ_{spec}	0.104	0.042
Γ_{diffuse}	0.013	0.168

Figures 10–12 show the forces that act on the tether–femtosatellite system. We expect the atmospheric drag force to be dominant for extremely small spacecrafts in LEO.[21] EDT thrust exceeds the drag force for a range of tether lengths. To increase the boosting capability, we choose a tether length where there is the greatest difference between the drag force and the EDT thrust. This length also corresponds to the length that minimizes required current (Fig. 8) and power (Fig. 9).

Figures 10–12 also reveal that the margin between EDT thrust and drag is small for each of the satellites. The margin can be widened by increasing the EDT current and utilizing a thinner tether. A thinner tether would lower the drag force at the expense of tether rigidity. We could increase the current by revisiting our assumptions and determining if the current collection model and available power estimate are too conservative.

It should also be noted that the gravity-gradient force is very small relative to other forces for the 10-mg satellite and the 1-g satellite. The gravity-gradient force generates tension along the tether and the torque aligns the tether along the local vertical. In this trade study, we assumed that the tether is aligned along the local vertical. For low inclination orbits, this alignment results in a maximum thrust given by Eq. (2). If we cannot assume vertical EDT orientation, the thrust should be calculated by Eq. (1). If the gravity gradient force is weak relative to the drag and solar pressure

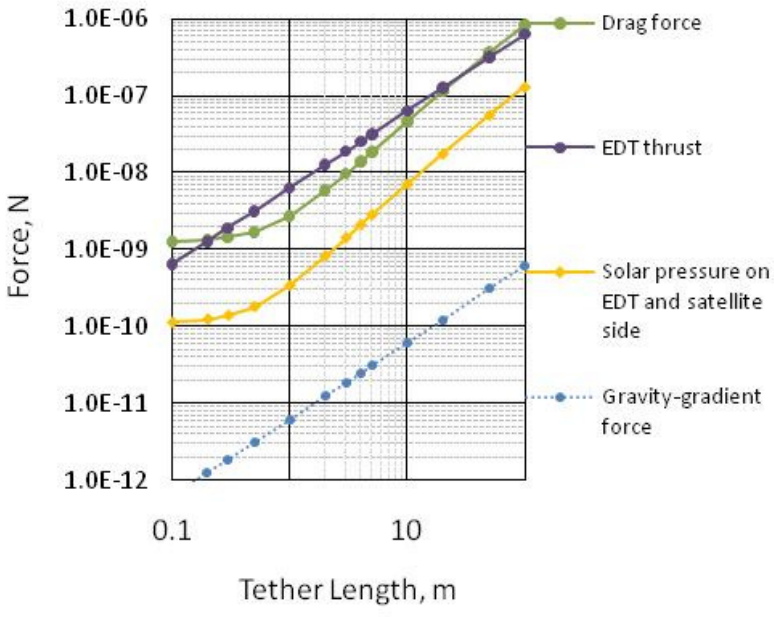

Figure 10. Forces on the 10-mg satellite and EDT.

forces, we cannot assume any orientation. The magnitude and direction of the resulting EDT force can vary widely so drag make-up is not guaranteed, even with sufficient tether current.

For the 100-g satellite using a 10-m EDT, the gravity-gradient force is about twice the drag force. We assume that the spacecraft is aligned along the local vertical for the 10-m EDT because the gravity-gradient force is dominant. We need to analyze the spacecraft dynamics in more detail to accurately estimate the orientation.

The gravity-gradient force is small for the 1-g satellite and negligible for the 10-mg satellite, so we cannot assume that the system is aligned along the local vertical. In order to use EDT propulsion for these satellites, we either need to implement an alternative method for ensuring vertical EDT alignment or we can utilize tethers oriented along multiple spacecraft axes, as proposed in Ref. 24. By orienting tethers along different axes, we may be able to provide EDT thrust without gravity-gradient stabilization. With multiple tethers on different axes, the satellite can boost regardless of its orientation.

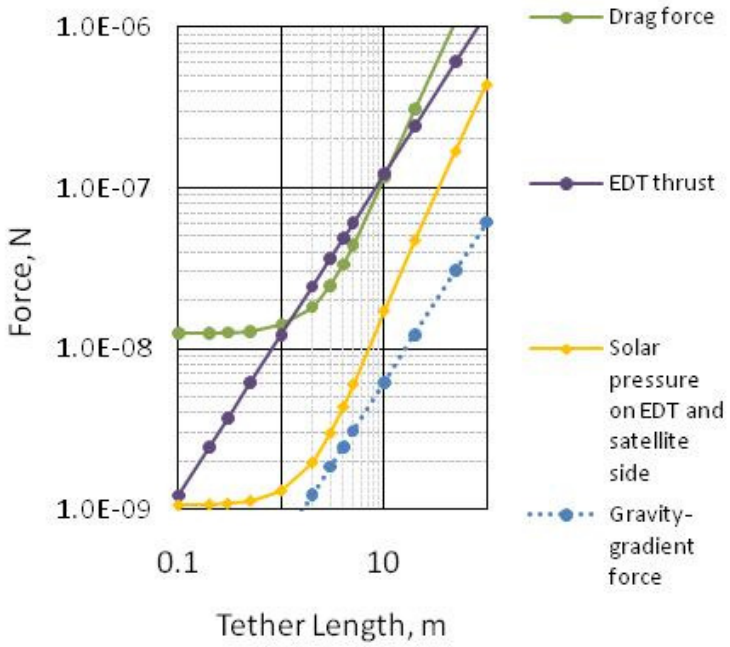

Figure 11. Forces on the 1-g satellite and EDT.

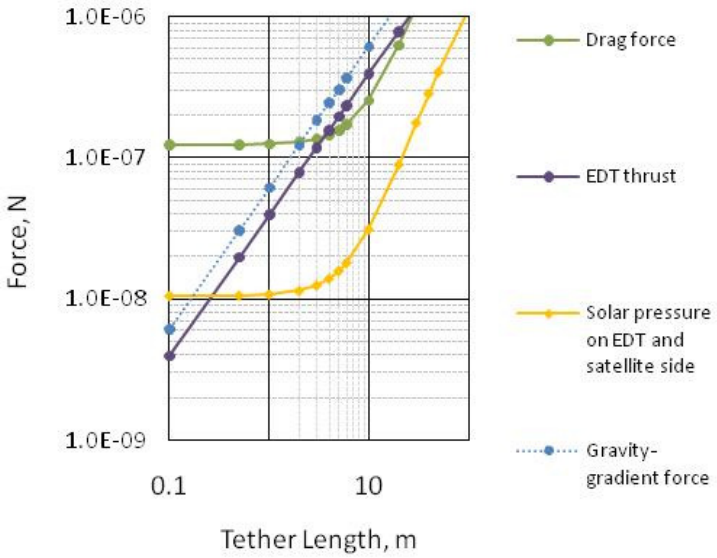

Figure 12. Forces on 100-g satellite and EDT.

J. Meteroidal and Orbital Debris

Micrometeroids and orbital debris pose a threat to tether missions in LEO. Estimates suggest that there are approximately 200 kg of meteoroids and around 1.5 million kg of manmade orbital debris orbiting at altitudes below 2000 km. Also, smaller size particles outnumber the large ones.[25] Thus, there is a much higher flux of particles equal to or bigger than the EDTs considered in this trade study than there are for conventional, larger diameter EDTs. It should be noted, however, that the small exposed surface area of the tethers reduces the probability of impact.

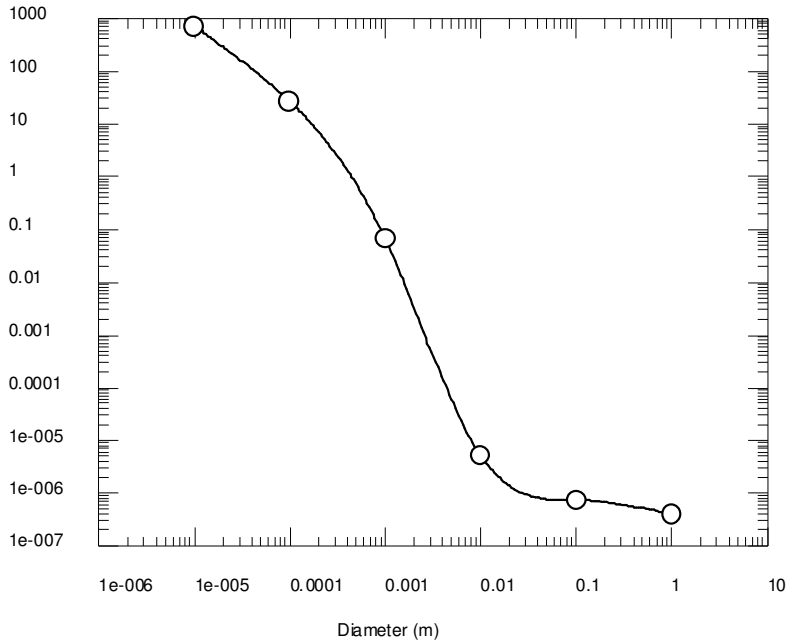

Figure 13. ORDEM2000 example output for flux at 500 km.

We used the NASA Orbital Debris Engineering Model (ORDEM-2000) to investigate this problem further. ORDEM calculated the flux of orbital debris between 10 µm to 10 m in diameter at a 500-km-circular altitude at 45° inclination in the year 2000, as shown in Fig. 11. We used this output to roughly estimate the probability of impact from particles with a diameter 1/3 the EDT diameter or greater in a 2-year period. It is a "rule of thumb" that particles 1/3 tether diameter can sever the tether.

There is also a need to explore other factors, like insulator degradation due to atomic oxygen, which may

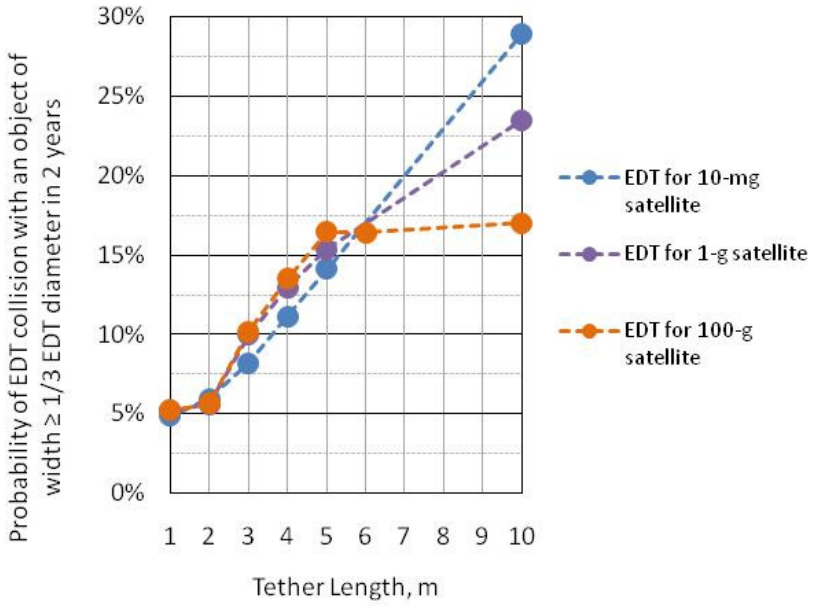

Figure 14. Probability of micrometeroid collision.

degrade tether performance over time.

III. Conclusion

A short, semi-rigid EDT scales to the small size needed, is propellantless, keeps the overall ChipSat mass low, and provides enough thrust to overcome drag in LEO. For low inclination orbits, the EDT's ability to provide thrust requires the tether to be oriented along or near the local vertical. The gravity-gradient force is large relative to other forces for the 100-g femtosatellite, so we assume the gravity gradient will align the tether. This assumption gives us confidence that the EDT system concept developed for the 100-g satellite has potential to enhance the maneuverability of the spacecraft.

The gravity-gradient force for the 10-mg and 1-g satellites is small relative to the drag and solar pressure forces, so we cannot conclude that the EDT thrust capability is possible for a single EDT. An array of short tethers oriented along different axes may be a feasible solution to EDT thrust for the small femtosatellites in the absence of gravity gradient stability. Table 6 highlights results from the trade study.

Table 6. Summary.

Parameter	10-mg Satellite	1-g Satellite	100-g Satellite
Satellite dimensions	1 mm × 1 cm × 1 cm	1 cm × 1 cm × 1 cm	2 cm × 5 cm × 5 cm
Ram drag cross sectional area	0.1 cm^2	1 cm^2	10 cm^2
EDT length	1 m	3 m	10 m
Tether diameter	24 µm	66 µm	212 µm
Tether mass	3 mg	80 mg	3 g
Available power (estimated)	13 mW	40 mW	600 mW
Current	214 µA	403 µA	1250 µA
Anode potential	17 V	52 V	430 V
Probability of collision with 1/3 size or larger debris in 2 years	5%	10%	17%
Is gravity gradient force significant?	no	no	yes

Appendix

Using D'Alembert's principle, one can transform an accelerating rigid body under external forces into a static system by adding inertial forces or torques that act through the center of mass of the object. We can then analyze the system as a static system under the influence of both external and inertial forces. Drag is the dominant perturbation force in LEO. We neglect the gravity-gradient and solar radiation pressure forces in this analysis for

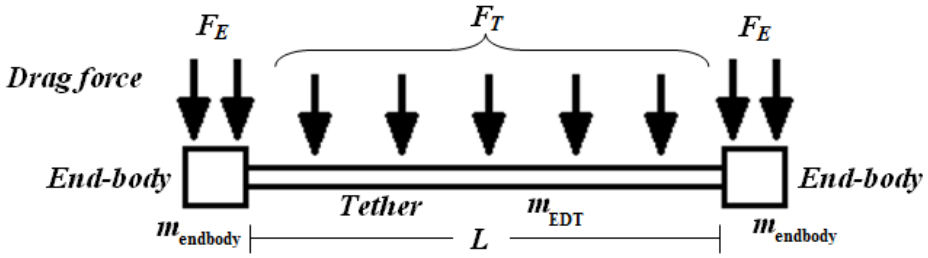

Figure 13. Drag force acting on the tether.

simplicity. Figure 13 shows the drag forces acting on the tether.

D'Alembert's principle can be written as

$$\sum_i \left(F_i - m_i a_{\text{accel},i}\right) \cdot \delta r_{d,i} = \delta W = 0 \,, \tag{26}$$

which allows us to conclude for an object in motion that

$$\sum_i \left(F_i - m_i a_{\text{accel,i}}\right) = 0 \,. \tag{27}$$

The applied force in Fig. 13 is all in the same direction. We can express the total acceleration due to the applied force as the ratio between this force and the total mass, given by

$$a_{\text{accel}} = \frac{\sum F}{\sum m} = \frac{F_T + 2F_e}{m_{\text{EDT}} + 2m_{\text{endbody}}} \,. \tag{28}$$

We write the inertial forces on the tether end-bodies as

$$F_{D,e} = m_{\text{endbody}} a_{\text{accel}} = m_{\text{endbody}} \left(\frac{F_T + 2F_e}{m_{\text{EDT}} + 2m_{\text{endbody}}} \right) \tag{29}$$

and on the tether

$$F_{D,T} = m_{\text{EDT}} a_{\text{accel}} = m_{\text{EDT}} \left(\frac{F_T + 2F_e}{m_{\text{EDT}} + 2m_{\text{endbody}}} \right) . \tag{30}$$

We can then find the difference between the applied and the inertial forces on the end-bodies, given by

$$F_{R,e} = F_e - m_e a_{\text{accel}} = F_e - m_{\text{endbody}} \left(\frac{F_T + 2F_e}{m_{\text{EDT}} + 2m_{\text{endbody}}} \right) \,, \tag{31}$$

which we can also express as

$$F_{R,e} = \left(\frac{F_e m_{\text{EDT}} - F_T m_{\text{endbody}}}{m_{\text{EDT}} + 2m_{\text{endbody}}} \right) . \tag{32}$$

The difference between the inertial and applied forces on the tether

$$F_{R,T} = F_T - m_{\text{EDT}} a_{\text{accel}} = F_T - m_{\text{EDT}} \left(\frac{F_T + 2F_e}{m_{\text{EDT}} + 2m_{\text{endbody}}} \right) \tag{33}$$

can be written as

$$F_{R,T} = -2 \left(\frac{F_e m_{\text{EDT}} - F_T m_{\text{endbody}}}{m_{\text{EDT}} + 2m_{\text{endbody}}} \right) = -2F_{R,e} \,. \tag{34}$$

The sum of the difference between applied and inertial forces is

$$F_{R,e} + F_{R,e} + F_{R,T} = 0 \,, \tag{35}$$

therefore satisfying Eq. (27).

Reframing the problem in Fig. 13 in terms of $F_{R,T}$ and $F_{R,e}$ allows us to solve the problem as a simple, static system shown in Fig. 14. We can now solve for the deflection of a simply supported beam with a distributed load w, where $w = F_{R,T}/L$. One should remember that the load $F_{R,T}$ distributed along the tether represents an imbalance in the actual force acting on the tether and the end-bodies. There is zero beam deflection when the $F_{R,T} = 0$, which means that the forces on the tether and end-bodies are balanced. However, the tether radii that ensure $F_{R,T} = 0$ would not be useful for our tether design, so we follow a different approach. The distributed load is given by

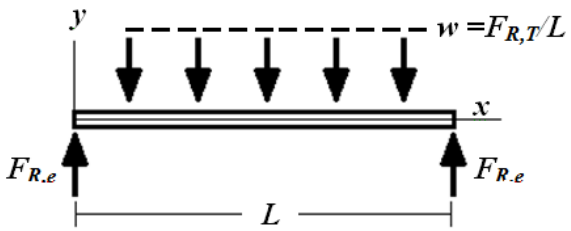

Figure 14. Simply supported beam with a distributed load *w*.

$$w = F_{R,T} / L \,. \tag{36}$$

The equation for the elastic curve of a beam is

$$\frac{\dfrac{d^2 y}{dx^2}}{\left[1 + \left(\dfrac{d^2 y}{dx^2} \right)^2 \right]^{3/2}} = \frac{M}{E\text{I}_{\text{inertia}}} \,, \tag{37}$$

which can be simplified for small curvature as

$$\frac{d^2 y}{dx^2} = \frac{M}{E\text{I}_{\text{inertia}}} \,. \tag{38}$$

The maximum deflection of a simply supported beam with an applied distributed load has a well known result, given by

$$y_{\max} = y(L/2) = \frac{-5wL^4}{384E\text{I}_{\text{inertia}}} \,. \tag{39}$$

Maximum deflection occurs at the beam center. We can define the maximum allowable deflection, $y_{\max}$, to be a small fraction of the overall tether length, expressed as

$$y_{\max} = \varepsilon L \,, \tag{40}$$

and we solve for the distributed force w that causes the deflection, giving us

$$w = \varepsilon \frac{384}{5} \frac{E\mathrm{I}_{\mathrm{inertia}}}{L^3}. \tag{41}$$

We expand the distributed force w to find the actual forces acting on the tether and the end-bodies, given by

$$-2\left(\frac{F_e m_{\mathrm{EDT}} - F_T m_{\mathrm{endbody}}}{m_{\mathrm{EDT}} + 2m_{\mathrm{endbody}}} \right) = \varepsilon \frac{384}{5} \frac{E\mathrm{I}_{\mathrm{inertia}}}{L^2}. \tag{42}$$

The drag force acting on the tether and the end-bodies is the product of the aerodynamic drag pressure and the area of the tether and the end-bodies. We can rewrite Eq. (42) as

$$P_{\mathrm{drag}} \left(A_{\mathrm{EDT}} m_{\mathrm{endbody}} - A m_{\mathrm{EDT}} \right) = \varepsilon 38.4 \frac{E\mathrm{I}_{\mathrm{inertia}}}{L^2} \left(m_{\mathrm{EDT}} + 2m_{\mathrm{endbody}} \right) \tag{43}$$

and rearrange the expression to get the pressure of aerodynamic drag

$$P_{\mathrm{drag}} = \varepsilon 38.4 \frac{E\mathrm{I}_{\mathrm{inertia}}}{L^2} \left(\frac{m_{\mathrm{EDT}} + 2m_{\mathrm{endbody}}}{A_{\mathrm{EDT}} m_{\mathrm{endbody}} - A m_{\mathrm{EDT}}} \right). \tag{44}$$

We assume that the insulator is thin and less rigid than the metal tether core and that the flexural rigidity, EI_{intertia}, of the entire tether can be represented by the flexural rigidity of the metal core. The radius of this core is $r - t_{\mathrm{in}}$, so the area moment of inertia of this core is

$$\mathrm{I}_{\mathrm{inertia}} = \frac{\pi}{4} \left(r - t_{in} \right)^4. \tag{45}$$

We can rewrite Eq. (44) as a function of radius and solve for the radius that causes the specified deflection

$$0 = \frac{1}{2} C_d \rho v^2 - \varepsilon 38.4 \frac{E\left(\frac{\pi}{4} \left(r - t_{\mathrm{in}} \right)^4 \right)}{L^2} \left(\frac{2m_{\mathrm{endbody}} + \left(\rho_{\mathrm{EDT}} L \pi \left(r - t_{\mathrm{in}} \right)^2 \right)}{2rLm_{\mathrm{endbody}} - A\left(\rho_{\mathrm{EDT}} L \pi \left(r - t_{\mathrm{in}} \right)^2 \right)} \right) \tag{46}$$

Acknowledgments

The authors gratefully acknowledge support from AFOSR grant FA9550-09-1-0646. I. C. Bell would also like thank J. Rager his enormous contribution to this study.

References

[1]Atchison, J. and Peck, M., "A Passive, Sun-Pointing, Millimeter-Scale Solar Sail," *Acta Astronautica*, Vol. 67, No. 1, pp. 108–121, 2010.

[2]Barnhart, D., Vladimirova, T., and Sweeting, M., "Very-small-satellite Design for Distributed Space Missions," *Journal of Spacecraft and Rockets*, Vol. 44, No. 6, 2007, pp. 1294–1306.

[3]Barnhart, D., Vladimirova, T., and Sweeting, M., "Satellite-on- a-chip Development for Future Distributed Space Missions," *Proceedings of the CANEUS Conference on Micro–Nano Technologies for Aerospace Applications*, Toulouse, France, 2006.

[4]Barnhart, D.J., "Very Small Satellite Design for Space Sensor Networks," Presentation, Brown University ChipSat Workshop, Providence, RI, Feb. 18, 2010.

[5]Peck, M. A., "A Vision for Milligram-scale Spacecraft," Presentation, Brown University ChipSat Workshop, Providence, RI, Feb. 18, 2010.

[6]Tang, W. C., "Overview of MEMS Programs at DARPA and Applications in Space," Presentation, First Canadian Workshop on MEMS Technology for Aerospace Applications, National Research Council, Canada, April 12, 2001.

[7]Bell, I. C., "Electrodynamic Tethers for ChipSat and Nanospacecrafts," Poster, Spacecraft Charging and Technology Conference, Albuquerque, NM, Sept. 23, 2010.

[8]Fuhrhop, K.R.P., "Theory and Experimental Evaluation of Electrodynamic Tether Systems and Related Technologies." Ph.D. Thesis, The University of Michigan, pp. 1–53, 2007.

[9]Larson, W. and Wertz, J. (eds.), *Space Mission Analysis and Design*, Microcosm, Inc., 1992.

[10]Willson, R. C., and A. V. Mordvinov, "Secular Total Solar Irradiance Trend During Solar Cycles 21–23," *Geophys. Res. Lett*., Vol. 30, No. 5, p. 1199, 2003.
[11]Hinkley, D., "Picosatellites at The Aerospace Corporation," Chapter 20 in *Small Satellites: Past, Present, and Future*, edited by H. Helvajian and S. W. Janson (The Aerospace Press and the AIAA, El Segundo, CA, 2009).
[12]Cosmo, M.L. and Lorenzini, E.C., "Tethers in Space Handbook," 2nd Ed., prepared for NASA/MSFC by Smithsonian Astrophysical Observatory, Cambridge, MA, 1989.
[13]Davis, J.R., *Nickel, Cobalt, and Their Alloys.* ASM International, Materials Park, OH, pp. 26–27, 2000.
[14]Dias, J.F., Bulla, A., and Yoneama, M.L., "Charging Effects in Thick Insulating Samples," *Nucl. Instr. and Meth*., Vol. B 189, 2002.
[15]Hibbeler, R.C., *Mechanics of Material*, 6th Ed., 2000, Prentice Hall International, Inc, Chaps. 6 and 12.
[16]Rubinstein, J. and Laframboise, J. G., "Theory of a Spherical Probe in a Collisionless Magnetoplasma" *Phys. Fluids*, Vol. 25, p. 1174, July 1982.
[17]Mott-Smith, H.M. and Langmuir, I. "The Theory of Collectors in Gaseous Discharges," *Phys. Rev*., Vol. 28, pp. 727–763, 1926.
[18]Parker, L W., and Murphy, B.L., "Potential Buildup on an Electron Emitting Ionospheric Satellite," *J. Geophys. Res*., Vol. 72, p. 1631, 1967.
[19]Whaley, D., *et al*., "100 W Operation of a Cold Cathode TWT," *IEEE Trans. Electron Devices*, Vol. 56, No. 5, pp. 896–905, May 2009.
[20]Warneke, B.A., *et al*., "An Autonomous 16 mm^3 Solar-powered Node for Distributed Wireless Sensor Networks," *IEEE Sensors 2002 Proceedings*, Vol. 2, p. 1510-1515, 2002.
[21]Kubo-oka, T. and Sengoku, A., "Solar Radiation Pressure Model for the Relay Satellite of SELENE," *Earth Planets Space*, Vol. 51, pp. 979–986, September 1999.
[22]Waters, D.L., Groh, K., Banks, B., and Cameron, K., "Changes in Optical and Thermal Properties of the MISSE 2 Peace Polymers and Spacecraft Silicones" International Symposium on Materials in a Space Environment, September 18, 2009.
[23]Atchison, J. and Peck, M., "Length Scaling in Spacecraft Dynamics," *Journal of Guidance, Control, and Dynamics*, Vol. 34, No. 1, pp. 231–246, 2011.
[24]Voronka, N., Hoyt, R.P., Gilchrist, B. E., and Fuhrhop, K., "An Architecture of Modular Spacecraft with Integrated Structural Electrodynamic Propulsion (ISEP)," NIAC 7 the Annual Meeting, Tucson, AZ, 18 October 2006.
[25]Tomlin, D.D., *et al*., "Space Tethers: Design Criteria," NASA Technical Memorandum 108537, Prepared by Structures and Dynamics Laboratory, Science and Engineering Directorate, MSFC Alabama, July 1997.